Title

Centrifuge Modeling of Variable-Rate Cone Penetration in Low-Plasticity Silts

Journal

Journal of Geotechnical and Geoenvironmental Engineering, 145(11)

ISSN

1090-0241

Authors

Price, AB
Boulanger, RW
DeJong, JT

Publication Date

2019-11-01

DOI

10.1061/(asce)gt.1943-5606.0002145

Peer reviewed

Centrifuge Modelling of Variable Rate Cone Penetration in Low-plasticity Silts

A. B. Price, M.ASCE[1], R. W. Boulanger, F.ASCE [2], and J. T. DeJong, M.ASCE [3]

[1]Corresponding Author, Fugro USA Land, Inc., Walnut Creek, CA, USA, a.price@fugro.com

[2]Professor, Department of Civil and Environmental Engineering, University of California, Davis, CA, USA

[3]Professor, Department of Civil and Environmental Engineering, University of California, Davis, CA, USA

Abstract

The effects of soil plasticity and penetration rate on cone penetration resistance in low-plasticity fine-grained soils are evaluated. A series of centrifuge tests with in-flight variable rate cone penetration soundings were performed on models of four slurry deposited mixtures of nonplastic silica silt and kaolin clay (0, 2.5, 5, and 20% kaolin by dry mass) with plasticity indices ranging from 0 to 6. Cone penetration resistances for an effective overburden stress of 100 kPa ranged from 260-400 atm (26-40 MPa) in the nonplastic silica silt to 4-18 atm (0.4-1.8 MPa) in the silt-clay mixture with a plasticity index of 6. The addition of a small amount of clay (as little as 2.5% by dry mass) to nonplastic silt resulted in an order of magnitude decrease in drained penetration resistance. Faster penetration rates produced partially drained and undrained conditions, with negative excess pores pressures developing in the nonplastic silica silt and positive excess pore pressures developing in the mixtures with 5% and 20% kaolin.

Introduction

Cone penetration resistance in fine-grained soils is dependent on the soil's compressibility, strength and dilatancy (which relate to state), and drainage conditions (relates to penetration rate for saturated soils), all of which can change significantly with small changes in the plasticity characteristics of the soil. The variation in cone penetration resistance with small changes in the plasticity characteristics of fine-grained soils is poorly understood, and yet has significant implications for the engineering procedures that are used for estimating monotonic or cyclic strengths.

Experimental studies of cone penetration in fine-grained soils have shown strong effects of both soil plasticity and cone penetration rate. Cone penetration resistance can increase or decrease with increasing penetration rate depending on the soil type and its state (e.g., state parameter or other measures of initial conditions relative to critical state). Rate dependency has been shown to normalize with the ratio of cone diameter to coefficient of consolidation, c_h, for (near) normally consolidated sedimentary clays where drained penetration resistances are about 2-3 times greater than undrained resistances and excess pore pressure generation is positive for penetration rates that produce partially drained and undrained conditions. This behavior is evident in the experimental cone penetration test results for sedimentary clays shown in Fig. 1(a) (from Randolph and Hope 2004, Silva et al. 2006, and Schneider et al. 2007 and 2008) that helped form the basis for the characteristic curve proposed by DeJong and Randolph (2012). In this figure, penetration resistance is expressed as the ratio of the normalized cone tip resistance, Q, and its reference value for undrained penetration, Q_{ref}, and the penetration rate is expressed as the normalized velocity, V. The normalized cone tip resistance is defined as

$$Q = \frac{q_t - \sigma_{vc}}{\sigma'_{vc}} \tag{1}$$

where σ'_{vc} is the vertical effective consolidation stress, σ_{vc} is the total vertical consolidation stress, and q_t is the total cone resistance, defined as

$$q_t = q_c + (1 - a)u_2 \tag{2}$$

where q_c is the measured cone resistance, a is the net area ratio, and u_2 is the pore pressure acting on the cone shoulder (Lunne et al. 1997). The normalized velocity is defined as

$$V = \frac{vd}{c_h} \tag{3}$$

where v is the penetration rate, d is the cone diameter, and c_h is the horizontal coefficient of consolidation. However, the normalized velocity values plotted in Fig. 1(a) were computed using the vertical coefficient of consolidation, c_v, because c_h values were not available. In contrast to the results for sedimentary clays in Fig. 1(a), Silva (2005) measured negative excess pore pressures and increased penetration resistances during partially drained and undrained penetration in nonplastic silica silt [Fig. 1(b)]. In this case, negative excess pore pressures generated from changes in shear stress are greater than the positive excess pore pressures generated by increased mean stress. The transition from essentially drained to essentially undrained penetration resistance typically occurs between normalized penetration velocities of 0.01 and 100 (Randolph 2004, DeJong and Randolph 2012) for sedimentary clays, which coincides with conditions often encountered during standard cone penetration testing (at a rate of 2 cm/s) in low to very low plasticity silts. Similar rate dependency was observed by Chow et al. (2018), Suzuki and Lehane (2014) and Jaeger et al. (2010) in centrifuge model tests on sand and sand with 25% kaolin. Chow

et al. (2018) found the transition from drained to partially drained penetration responses to coincide with a normalized penetration velocity of about 7, with penetration resistances generally decreasing in loose sand and increasing in dense sand with increasing penetration rate. Suzuki and Lehane (2014) found penetration conditions to transition from undrained to partially drained at $V \approx 10$ and from partially drained to drained at $V \approx 0.1$ for sand with 25% kaolin (PI = 6.3), with drained penetration resistances about 8.6 times greater than undrained penetration resistances (i.e., $Q_{drained}/Q_{undrained} \approx 8.6$). Jaeger et al. (2010) observed similar trends in a centrifuge model test on sand with 25% kaolin but with $Q_{drained}/Q_{undrained} \approx 17$. Suzuki and Lehane (2014) also performed in-flight cone penetration testing in sand with 10% kaolin (PI = 3.8); penetration appeared to be drained for the range of penetration rates they tested ($V \leq 0.2$), with drained penetration resistances about 67% greater than measured in the sand with 25% kaolin. The range of penetration resistances measured in these studies vary in magnitude from a few atmospheres (<1 MPa) for kaolin (aligning with empirical expectation based on undrained strength normalization relationships for clays) to greater than 500 atmospheres (50 MPa) for partially drained penetration in nonplastic silica silt.

The monotonic and cyclic undrained strengths of fine-grained soils or sands with high fines contents are commonly estimated using engineering procedures that were developed either for clays and plastic silts or for nonplastic silts and sands, neither of which provides adequate resolution for low or very low plasticity soils that do not fall clearly into either group. For example, the case history-based liquefaction triggering correlation for cohesionless or sand-like soils by Boulanger and Idriss (2016) allows for the effects of nonplastic fines, but the case history database lacks sufficient detail to distinguish between purely nonplastic fines and fines of very low plasticity [e.g., a plasticity index (PI) less than 4 or 5 is close to the limit of what is often measurable]. The

variation in cone penetration resistance with fines content for the same cyclic resistance ratio (CRR) for this correlation is plotted in Fig. 2, showing that increasing fines content is expected to reduce cone penetration resistance in soils with similar CRRs. The q_{c1N} (penetration resistance in atmospheres at a σ'_{vc} of 1 atmosphere) at high fines contents, however, are much greater than would be obtained in more plastic silts and clays, illustrating the lack of resolution for soils of intermediate plasticity.

The present study examines cone penetration resistance in low-plasticity, fine-grained soils, with a focus on the effects of small changes in plasticity characteristics (or clay content) and penetration rate. A series of 1-meter radius centrifuge tests was performed with centrifugal accelerations of 80 g and 105 g to evaluate the effects of penetration velocity and soil compressibility on penetration resistance for slurry deposited mixtures of silica silt and kaolin clay. In-flight cone penetration soundings were performed at penetration velocities ranging from 0.01 mm/s to greater than 100 mm/s with a 6-mm diameter cone penetrometer in centrifuge models of slurry deposited silt-clay mixtures with PIs ranging from 0 to 6 (0, 2.5, 5, and 20% kaolin). First, laboratory characterization of the low-plasticity silt mixtures is presented, including results from high stress one-dimensional compression testing. Second, construction of the centrifuge models is described. Third, corrections applied to measured cone resistances to account for pore pressures acting on the cone shoulder and temperature gradients in the models are described and results from in-flight T-bar penetration tests for the PI = 6 (20% kaolin) mixture are presented. Fourth, results from five centrifuge tests on the silt-clay mixtures are presented and examined. Last, experimental limitations and practical implications are discussed. Experimental studies such as the one presented herein can provide a basis for the development of theoretically informed interpretation methods

by providing (1) systematic variation of key conditions/behaviors/properties and (2) more complete material characterization than is typical of most site characterization programs.

Low-plasticity Silt Mixtures and their Characteristics

Four mixtures of nonplastic silica silt and kaolin clay with PIs ranging from 0 to 6 were used in this study. The nonplastic silica silt (U.S. Silica SIL-CO-SIL 250) was crushed and highly angular with a median particle size of approximately 50 microns. The kaolin clay was Old Hickory No. 1 Glaze and had a liquid limit (LL) = 58.9 and PI = 33. Mixtures were prepared with 0, 2.5, 5 and 20% kaolin by dry mass and are referred to herein as 100S, 97.5S2.5K, 95S5K, and 80S20K, respectively. The 80S20K had a PI of 6 while the other three mixtures were nonplastic (PI = 0). While not used in the study presented herein, mixtures with 10% kaolin (90S10K) were found to have a PI of approximately 1.

Specimens for laboratory element testing were prepared by a slurry mixing and sedimentation process. Slurries were mixed under vacuum by a propeller mixing blade and mechanical rotation of a cylindrical mixing chamber as described by Krage et al. (2018) and Price et al. (2017). The 100S silt was mixed at a water content of 29.6%, the 97.5S2.5K and 95S5K mixtures were both mixed at a water content of 35%, and the 80S20K (PI = 6) mixture was mixed at a water content of 44.6% (twice its liquid limit).

Results from one-dimensional compression tests with vertical stresses exceeding 100 MPa for slurry deposited specimens of the low-plasticity silts are shown in Fig. 3. Compression curves in void ratio versus log vertical effective stress (σ_v') space are shown in Fig. 3(a). At a σ_v' of 100 kPa, the 100S silt was more dense (smaller void ratio) than the other three silt-clay mixtures. Volumetric strains from a reference stress of σ_v' = 100 kPa are plotted versus σ_v' in Fig. 3(b). The

silt-clay mixtures exhibited increased compressibility with increasing clay content. The 97.5S2.5K and 95S5K mixtures behaved similarly; they were more compressible than the 100S silt and significantly less compressible than the 80S20K mixture. The shape of the compression curves transitions from that typical of nonplastic soils (an initially stiff response followed by increased compressibility often associated with particle/asperity crushing as σ_v' exceeds 30 MPa) to that typical of clay-like soils (linear response over the range of stresses typically tested for clays) as clay content is increased.

Values of c_v for the 80S20K mixture and 100S silt were estimated from constant rate of strain (CRS) and incremental load (IL) consolidation test results (Krage et al. 2018; Krage 2018, personal communication). Estimates of c_v were made from test results for normally consolidated, slurry deposited specimens for σ_v' = 100-300 kPa. Values of c_v for the 97.5S2.5K and 95S5K mixtures were assumed equal based on a limited number of IL consolidation tests (Haugaard et al. (2018)), which were consistent with values interpolated from CRS consolidation test results for the other mixtures. The values used herein are: $c_v = 1 \cdot 10^{-5}$ m^2/s for the 100S silt; $c_v = 8.5 \cdot 10^{-6}$ m^2/s for the 97.5S2.5K and 95S5K mixtures, and $c_v = 3 \cdot 10^{-6}$ m^2/s for the 80S20K mixture. The horizontal coefficient of consolidation was estimated as twice the value in the vertical direction ($c_h \approx 2 \cdot c_v$).

Undrained monotonic direct simple shear (DSS) test results for slurry deposited specimens of the 100S silt and 80S20K mixture for three levels of confinement are shown in Fig. 4. Stress paths and stress-strain responses are shown for the 100S silt and 80S20K mixture in Figs. 4(a and b) and Figs. 4(c and d), respectively. The 100S silt exhibits dilative tendencies at large shear strains for the range of initial conditions tested (σ_{vc}' = 100, 800, 1600 kPa) indicating initial states that are

dense of critical state (negative values of the state parameter). Conversely, the 80S20K mixture exhibits undrained strength normalization and contractive tendencies for the range of initial conditions tested (σ'_{vc} = 100, 400, 800 kPa), indicating initial states that are loose of critical state (positive values of the state parameter). It can be reasonably inferred that initial slurry deposited states for the two intermediate mixtures (97.5S2.5K and 95S5K) lie somewhere between the initial states of the two bounding mixtures (100S and 80S20K), although additional DSS testing would be required to confirm this inference.

Additional details on the testing procedures and results are presented by Price (2018) including grain size distributions, monotonic and cyclic DSS test results and scanning electron microscope images. The experimental data for the one-dimensional compression and consolidation tests and all DSS tests are available in Haugaard et al. (2018) and Price et al. (2018b).

Description of Centrifuge Models

Five centrifuge model tests with in-flight cone penetration soundings were performed using the 1-m radius geotechnical centrifuge at the Center for Geotechnical Modelling at the University of California, Davis. Tests were performed at a centrifugal acceleration of 105 g (unless otherwise noted) using a 38 cm x 38 cm x 24 cm deep rigid container. Two models were constructed for the 80S20K mixture (one of which was tested at 80 g) and one model was constructed for each of the other three soils (100S, 97.5S2.5K, 95S5K). Cross-sectional and plan views of the typical centrifuge model configuration are shown in Fig. 5. Penetration resistance was measured at the 60° conical tip of the 6-mm diameter instrumented cone penetrometer while the load cell positioned between the actuator and the head of the penetrometer provided an additional measurement of resistance that included the resistance along the shaft of the penetrometer. All

penetration resistances presented herein are tip resistances measured at the instrumented tip. A Monterey sand drainage layer was placed on the container floor with a sheet of filter paper separating it from the overlying silt or silt-clay mixtures. Pore pressure transducers were placed at approximately mid depth of the silt/silt-clay layer and used to monitor model consolidation. The water surface was maintained approximately 3 cm above the soil surface throughout testing to limit temperature changes of the cone by keeping the cone tip submerged throughout testing. Following initial in-flight model consolidation and prior to each cone sounding the model was spun up to the desired g level (generally 105 g) and allowed to reconsolidate. Following each cone push, the model was spun down and the cone actuator position manually changed. There were eight planned cone soundings for each model though most models involved additional soundings in between the planned locations. The pore fluid was deionized water for all tests. All data are presented in model units following the approach adopted by Silva (2005). Dimensionless normalized velocity values are equivalent when computed in either model or prototype scales following the standard scaling relationships for modelling diffusion processes (e.g., Kutter et al. 1995). The experimental data presented herein are archived in Price et al. (2018a).

The silt and silt-clay mixtures were slurry deposited into the rigid container following placement of the sand drainage layer and filter paper. Slurries were mixed under vacuum in a modified cement mixer; slurry deposition was chosen to provide common preparation across the four soils tested while maintaining uniform mixtures of the binary constituents. Initial fabric of the slurry deposited soils is thought to be analogous to that found in fluvial depositional environments. Photos of slurry preparation and model construction are shown in Fig. 6. The 100S silt was poured directly from the mixer down an open channel into the container [Fig. 6(f)] while the other silt-clay mixtures were spooned into the container [Figs. 6(d and e)]. The 6-mm diameter cone

penetrometer and the actuator and actuator rack used to position and push the cone are shown in Figs. 6(g and h).

In-flight cone penetration was performed at penetration velocities ranging from 0.01 mm/s to greater than 100 mm/s (which corresponds to V ranging from 0.003 to greater than 100 across the four soils). The cone penetrometer had a capacity of 100 lbf (445 N) and was not instrumented with a pore pressure transducer for measuring pore pressures acting on the cone shoulder. Cone soundings were spaced at least 10 cm from container walls and initially at least 6 cm (10 cone diameters) apart, though additional cone soundings (supplemental to those shown in Fig. 5) were in closer proximity to prior sounding locations. Bolton et al. (1999) showed that side boundary and container size effects were minimal for cone soundings approximately 10 or more cone diameters from the nearest container wall and container to cone diameter ratios exceeding about 30, respectively, for centrifuge cone penetration tests in a uniform silica sand. Some of the cone soundings were performed at multiple penetration rates. Cone penetration soundings targeting slow rates were initially pushed at a faster rate to advance the cone to the target depth interval (generally for determination of penetration resistance at σ'_{vc} = 80 to 100 kPa). For dual rate soundings, time was allowed between advancing the cone at the different rates to allow for pore pressures that may have been generated during the initial (faster) push to dissipate prior to beginning penetration at the target slow rate.

Two T-bar penetration tests were performed in the 80S20K (PI = 6) mixture to obtain independent measurements of undrained shear strength, s_u, to compare with cone penetration test results and laboratory DSS test results for the same mixture. T-bar soundings consisted of 10 penetration cycles at 10 mm/s providing measurements of the initial and remolded undrained strengths. Following initial penetration to a depth of 123 mm, the T-bar was cycled between depths

of 63 and 113 mm. The T-bar had a shaft diameter of 6 mm, a bar diameter of 7 mm and a bar length of 40 mm. The T-bar was instrumented with a strain gauge load cell to measure penetration resistance at the base of the shaft just behind the bar. The T-bar penetration rate (10 mm/s) was selected to achieve undrained penetration in the 80S20K mixture based on (1) normalized velocities for undrained penetration of the 6-mm diameter cone penetrometer in the same mixture and (2) results from T-bar penetration test results in reconstituted Burswood Clay presented by Chung et al. (2006).

Corrections to Cone Penetration Resistances and Comparison to T-bar Results

Measured cone penetration resistances were corrected for two effects: (1) pore pressures acting on the cone shoulder behind the tip and (2) temperature changes during penetration. The correction for pore pressures acting on the cone shoulder is standard in practice but is complicated by the lack of pore pressure measurements for the cone soundings in the centrifuge models. Changes in temperature during cone penetration can shift the effective zero of the cone tip load cell; this effect can be significant if the change in temperature is large and/or if the measured loads are small. The corrections made to account for these two effects and associated assumptions are described in this section.

A pore pressure correction accounting for excess pore pressure generation during cone penetration was applied to cone soundings where $V > V_{50}$ where V_{50} is the normalized penetration velocity at which the cone penetration resistance is half way between the fully drained and undrained values. This correction was only applied to account for excess pore pressure generation for cone soundings in the 80S20K and 95S5K mixtures because they exhibited (1) undrained penetration resistances that were multiple times smaller than drained resistances indicating

generation of positive excess pore pressures during undrained and partially drained penetration and (2) small undrained penetration resistances making them particularly sensitive to the correction as is discussed subsequently. The total cone resistance, q_t, was computed from the measured cone resistance, q_c, accounting for pore pressures acting on the cone shoulder as illustrated in Fig. 7 and described by Eq. (2). A net area ratio of a = 0.62 was used to estimate the magnitude of the correction based on measurements from calibration chamber tests. An assumption regarding the magnitude of excess pore pressure generated at the cone shoulder was necessary to account for such effects on the measured penetration resistance. The value of the pore pressure parameter, B_q, was taken to be 1 for the 80S20K and 95S5K mixtures where B_q is defined as

$$B_q = \frac{u_2 - u_o}{q_t - \sigma_{vc}} \tag{4}$$

where $u_2$is the pore pressure at the cone shoulder, u_o is the initial hydrostatic pore pressure, q_t is the total cone resistance, and σ_{vc} is the total vertical consolidation stress. This B_q value was selected based on empirical data for soft, normally consolidated clays (i.e., Robertson 1990, Schneider et al. 2008). A B_q value in the upper range of the empirical data was considered appropriate given (1) the large ratios of drained to undrained penetration resistance measured for the 80S20K and 95S5K mixtures, (2) the small undrained shear strengths measured for the 80S20K mixture by laboratory DSS tests and (3) the collapsible structure these results suggest for young, slurry deposited specimens. For all other penetration rates ($V < V_{50}$) and for the other soils (100S and 97.5S2.5K for all values of V) the pore pressure correction was applied with B_q = 0, only accounting for hydrostatic pore pressures acting on the cone shoulder.

A temperature correction was applied to all cone soundings to account for the effects of temperature variation during cone penetration on cone tip resistance measurements. The temperature sensitivity of the cone penetrometer was measured at 1 g in a calibration water bath for temperatures ranging from 33 to 116°F. The measured variation of the cone tip load with temperature is well approximated by a linear fit with a sensitivity of 11.7 N/°F which when projected over the cone area is 41.4 kPa/°F. A linear temperature differential of 2°F between the soil surface and the bottom of the cone soundings was assumed (with the temperature assumed to be greater at the soil surface) and resulted in a maximum increase in penetration resistance (at the bottom of the cone soundings) of 83 kPa. In the absence of direct temperature measurements to constrain this correction, the described approach was adopted because it is simple and thought to be reasonable. Conditions during model testing suggested that ambient temperature in the centrifuge chamber changed significantly due to both heat generation from spinning and daily fluctuation of ambient room temperature. Temperature changes at these time scales may have developed temperature gradients in the centrifuge models causing the temperature of the cone tip (where strain gauges to measure load are instrumented) to fluctuate during penetration. Temperature changes from frictional heat generation during cone penetration were not explicitly considered as they were expected to be negligible given the small penetration resistances. Careful attention was also paid to determination of the load cell zero as the measured loads were only 1-2% of the load cell's capacity for undrained penetration in the 80S20K and 9525K mixtures.

The effects of the applied corrections for a typical cone sounding at an undrained penetration rate in the 80S20K mixture are shown in Fig. 8. The magnitude of the temperature correction is shown by the difference between profiles of raw measured cone tip resistance, q_{c_raw}, and the temperature corrected value, q_c. The pore pressure correction is shown by the difference

between profiles of q_c and q_t. Undrained penetration resistances in the 80S20K and 95S5K mixtures were most sensitive to the applied corrections because of their small magnitude.

T-bar penetration soundings were performed in the 80S20K mixture to establish the dependence of penetration resistance on undrained shear strength without the uncertainties associated with the cone penetrometer. Results from these tests are consistent with laboratory element DSS test results and empirical variation of undrained strength with overconsolidation for sedimentary clays, as discussed below. Results from T-bar soundings for overconsolidation ratios (OCRs) of 1 and 2 are plotted in Fig. 9. T-bar measurements were corrected for drift (likely associated with temperature changes and bending) based on the cyclic offset for remolded conditions (i.e., the difference between penetration and extraction resistances for the final loading cycle) and external load cell measurements. Both T-bar soundings were in the same centrifuge model; the normally consolidated sounding was performed at 105 g, whereas the overconsolidated sounding was performed at 53 g after prior consolidation at 105 g. T-bar net penetration resistance ($q_{T-bar,net}$) profiles are plotted in Fig. 9(a) where $q_{T-bar,net} = q_{T-bar} - [\sigma_{vc} - u_o(1-\alpha)]\frac{A_s}{A_p}$ and q_{T-bar} is the T-bar penetration resistance, α is the ratio of the T-bar load cell core area to the T-bar shaft area ($\alpha = \frac{(4.7\text{mm})^2}{(6\text{mm})^2} = 0.61$), A_s is the T-bar shaft area, and A_p is the projected area of the T-bar tip. The difference in the vertical effective stress range for the two soundings stems from the difference in g-level. For both soundings, the T-bar was cycled up and down 10 times at a rate of 10 mm/s. Both soundings exhibit a reduction in penetration resistance from remolding of the soil as the T-bar is cycled. Soil remaining on the top of the T-bar after testing is one cause for the apparent offset in the T-bar penetration resistance in Fig. 9. Profiles of undrained strength ratio, s_u/σ'_{vc}, are plotted in Fig. 9(b) where the undrained strength is computed using the empirical

correlation $s_u = q_{T-bar,net}/N_{T-bar}$ where N_{T-bar} is the T-bar strength factor and is taken to be 10.5 in the present analysis (White et al. 2010, DeJong et al. 2011). Average strength ratios over a common vertical effective stress interval (25-60 kPa) are indicated by grey vertical lines with values of $(s_u/\sigma'_{vc})_{\mathrm{OCR}=1}$ = 0.14 and $(s_u/\sigma'_{vc})_{\mathrm{OCR}=2}$ = 0.24. The variation of undrained strength with overconsolidation is often expressed by the empirical expression $(s_u/\sigma'_{vc})_{\mathrm{OCR}} = (s_u/\sigma'_{vc})_{\mathrm{OCR}=1} \cdot \mathrm{OCR}^m$, where parameter m is typically taken to be 0.8 for sedimentary clays. Undrained monotonic DSS tests results for slurry sedimented specimens of the 80S20K mixture with OCR = 1, 4 and 8 produced a m value of 0.70 [s_u/σ'_{vc} = 0.16, 0.43 and 0.69 for OCR = 1, 4, and 8, respectively; corresponding experimental data is presented by Price (2018)]. The T-bar measured strength ratios produce m = 0.78, although values ranging from 0.7 to 0.9 can be reasonably computed depending on the depth interval used for averaging. The T-bar measured strength ratios are reasonably consistent with both element test results and empirical expectation; weaker normally consolidated undrained strength ratios measured by both T-bar soundings and DSS tests (relative to the 0.22 value typical for sedimentary clays) may partly reflect the young age of the slurry deposited specimens.

Cone Penetration Test Results

Results from the in-flight variable rate cone penetration test soundings are presented in this section. All cone penetration resistances are corrected as described in the previous section unless otherwise indicated. Profiles of normalized total cone penetration resistance versus vertical effective consolidation stress are shown in Fig. 10 (note that σ'_{vc} = 100 kPa corresponds to a model depth of approximately 9.2 cm for tests performed at 105 g). Triangles indicate the start of target push intervals for dual penetration rate soundings. The shade of the cone penetration resistance profiles corresponds to the penetration rate. The 100S silt exhibited increasing penetration resistance with

increasing penetration rate for penetration velocities exceeding approximately 0.01 m/s [Fig. 10(a)]. This behavior is consistent with Silva's (2005) findings for nonplastic silt and suggests generation of negative excess pore pressures during partially drained and undrained penetration. Increases in penetration resistance with penetration rate were greater near the soil surface, which may reflect variation in model density, fabric, and/or drainage condition stemming from depositional variation and/or increasing confinement with depth. Such surface behavior may also be partly attributable to ageing effects and increased dilatancy at low confinement. For penetration rates less than approximately 0.01 m/s, cone profiles are similar for vertical effective stresses exceeding 30 kPa; this suggests penetration is drained at these rates. Penetration resistances in the 97.5S2.5K mixture [Fig. 10(b)] were roughly an order of magnitude less than those measured in the 100S silt (note the difference in penetration resistance scales in Fig. 10) and exhibited a more variable rate dependency. Variability within and across the measured cone profiles in this mixture suggest that it may be near the threshold for changes in behavior. Small variations in clay content, fabric, density, or state within the model may transition behavior from predominately dilative to contractive and/or from drained to partially drained or undrained. The two other mixtures (95S5K and 80S20K) exhibited decreasing penetration resistance with increasing penetration rate [Figs. 10(c and d)]. This behavior suggests generation of positive excess pore pressures during partially drained and undrained penetration such as is expected for near normally consolidated clays or clayey silts. Multiple dual rate pushes with slow target penetration rates were required to establish close to drained penetration in the 80S20K mixture. Cone penetration profiles for the 80S20K mixture terminate at different maximum vertical effective consolidation stresses because of the different g-levels the models were tested at (one was at 80 g and one was at 105 g).

Raw and corrected penetration resistances (q_{cN_raw}, q_{cN} and q_{tN}) at σ'_{vc} = 80 kPa for the 80S20K (PI = 6) mixture are plotted versus cone velocity in Fig. 11. The applied corrections for temperature (from q_{cN_raw} to q_{cN}, where $q_{cN} = q_c/P_a$ and P_a is the atmospheric pressure) and pore pressures acting on the cone shoulder (from q_{cN} to q_{tN}) are most significant for undrained penetration rates as previously discussed. For drained and partially drained penetration rates with $V < V_{50}$, the differences between q_{cN} and q_{tN} reflect only hydrostatic pore pressures acting on the cone shoulder (i.e., $B_q = 0$ is assumed). Undrained q_{tN} values of approximately 3.0 (0.3 MPa) at σ'_{vc} = 80 kPa (and σ_{vc} = 180 kPa, recalling there was 3 cm of water above the soil surface) correlate to a cone strength factor, N_{kt}, of 11.1 given the normally consolidated undrained strength ratio s_u/σ'_{vc} = 0.14 determined from the T-bar penetration soundings (whereas s_u/σ'_{vc} = 0.16 from DSS lab tests) and the relationship $s_u = (q_t - \sigma_{vc})/N_{kt}$. Empirical data for clays supports N_{kt} values ranging from 10-20, with N_{kt} = 15 on average. Uncertainty in the applied corrections (no pore pressure or temperature measurements) makes comparison of N_{kt} values to empirical data sets difficult; however, even given this uncertainty there is reasonable consistency between the cone penetration test results, the T-bar penetration test results, and the undrained monotonic DSS test results.

Penetration resistances at σ'_{vc} = 80 and 100 kPa for all four silts are plotted versus absolute and normalized penetration velocities in Figs. 12 and 13, respectively. These figures use logarithmic y-axes (Q *and* Q/Q_{ref}) to distinguish behaviors of the three silt-clay mixtures (97.5S2.5K, 95S5K, 80S20K) which generally exhibit penetration resistances an order of magnitude smaller than those measured in the 100S silt. The trend lines plotted in these figures follow the form suggested by DeJong and Randolph (2012) where

$$Q = Q_{undrained} + \frac{Q_{drained} - Q_{undrained}}{1 + \left(\frac{V}{V_{50}}\right)^{c}} \quad (5)$$

where Q is replaced with q_{tN} and V with absolute cone velocity, v, for the trends shown in Fig. 12. Parameter c, which describes the rate of change of penetration resistance with velocity, was constrained to a value of 1 (the value DeJong and Randolph use in their characteristic curve for near normally consolidated clays) for the mixtures with kaolin because of limited data in the transition zone. Separate trends for σ'_{vc} = 80 kPa and 100 kPa are shown in Fig. 12; trends in Fig. 13 are for data points at both stress levels because values of Q are normalized for overburden stress. The two trends (shown as dashed lines) in Fig. 13 for the 97.5S2.5K mixture were selected to represent the range of expected behavior given the variability of penetration resistance with velocity.

Comparison of centrifuge cone penetration velocities to the standard field rate of 0.02 m/s can be made through equivalency of normalized velocity. A standard 15 cm^2 cone pushed at 0.02 m/s has a normalized velocity equivalent to a 6-mm diameter cone pushed at 0.146 m/s in the same soil. The trend lines plotted in Fig. 12 suggest that this penetration rate corresponds to undrained penetration in the 80S20K and 95S5K mixtures, and undrained or partially drained penetration in the 97.5S2.5K mixture and 100S silt. This equivalent penetration velocity (0.146 m/s) coincides with normalized velocities of 44, 52, 52, and 146 for the 100S, 97.5S2.5K, 95S5K and 80S20K soils, respectively.

Differences in the penetration resistance magnitude and characteristics of pore pressure generation during partially drained and undrained penetration between the four soils are evident in Fig. 13. Drained and undrained penetration resistances generally increase as clay content

decreases, with the most significant change in penetration resistance occurring between the soils with 0 (100S) and 2.5% (97.5S2.5K) clay. The 80S20K and 95S5K mixtures show variation of penetration resistance with penetration velocity consistent with positive pore pressure generation during undrained penetration (where undrained penetration resistances are less than drained resistances). The normalized ratio of drained to undrained penetration resistance, $Q_{rat} = Q_{drained}/Q_{undrained}$, is 8.8 and 4.4 for the 80S20K and 97.5S2.5K mixtures, respectively. These values are greater than the range of 2 to 3 reported by DeJong and Randolph (2012) for near normally consolidated clays but smaller than the value of 17 reported by Jaeger et al. (2010) for young, very soft, slurry sedimented, normally consolidated clayey sand. The 100S silt exhibits the opposite trend, with behaviors indicative of negative excess pore pressure generation during undrained penetration (where partially drained and undrained penetration resistances are greater than drained penetration resistances). These behaviors are consistent with the differences in initial state (relative to critical state) implied by the undrained monotonic DSS test results for slurry deposited specimens of the 100S silt and 80S20K mixture presented in Fig. 4. The scattered data points for the 97.5S2.5K mixture for $V > 1$ likely reflect model variations near the threshold where (1) pore pressure generation characteristics vary between positive and negative excess pore pressure generation during undrained penetration and (2) drainage characteristics vary between drained, partially drained, and undrained for a given penetration rate (i.e., local variations in kaolin content may cause drainage during penetration a given rate to vary throughout the model).

Normalized penetration resistance at σ'_{vc} = 100 kPa is plotted versus percent kaolin in Fig. 14 for normalized penetration velocities ranging from 0.01 to 100. The data points in this figure are from the Q-V relationships shown on Fig. 13. Note that normalized velocities increase for a given penetration velocity as clay content increases and c_h decreases. The order of magnitude

reduction in penetration resistance with the addition of a small amount of plastic fines to the nonplastic silica silt (from 100S to 97.5S2.5K) outweighs differences in penetration resistance caused by rate effects [i.e., the difference in penetration resistance between mixtures with 0% and 2.5% kaolin is much greater than the variation of penetration resistance with penetration rate (for V = 0.01-100) for either mixture].

Discussion

Conceptually, increasing kaolin content can increase soil compressibility and decrease permeability as well as alter the slurry deposited state and strength-dilatancy behavior of the silt-clay mixtures. Separating the relative contributions of these changes to changes in cone penetration resistance is challenging. The experimental work presented herein offers insight in this regard, but further testing and numerical analyses are necessary. Similar state-CRR and state-dilatancy behavior for the 100S and 80S20K soils can be inferred from experimental DSS tests by Price et al. (2017); therefore, differences in dilative tendency and friction angle may largely stem from differences in slurry deposited state. At low clay contents, the kaolin may partially coat silica particles causing a loose and potentially collapsible slurry deposited structure to develop. Increasing state (increasing void ratio relative to critical state) with increasing kaolin content for the slurry deposited silt-clay mixtures is consistent with this conceptual interpretation and the undrained monotonic DSS test results for the 100S and 80S20K soils.

An order of magnitude decrease in drained penetration resistance was observed with the addition of a small amount of plastic fines to the nonplastic silt (from 100S to 97.5S2.5K) with a negligible change in fines content. Partially drained and undrained tip resistance decreased even more substantially (than drained resistance) with the addition of plastic fines to the nonplastic silt.

This sharp decrease in tip resistance suggests that cone penetration resistance in nonplastic and very low-plasticity silts alone may not be a reliable predictor of monotonic and cyclic strengths. This change in penetration resistance with small changes in clay content is conceptually consistent with (1) differences in one-dimensional compressibility, (2) differences in initial slurry deposited state and associated differences in dilative tendency and friction angle, and (3) evolving magnitude and sign of excess pore pressure generation during partially drained and undrained penetration, though the relative contributions of such variations to the observed changes in penetration resistance is unclear from the test results presented herein. Numerical simulation can provide insight in this regard through exploration of penetration resistance in these silt-clay mixtures across a wider range of initial conditions. For example, it is expected that differences in penetration resistance between the 100S and 97.5S2.5K soils would be less if prepared at similar states.

The drained penetration resistance measured for the slurry deposited nonplastic silt (100S) is substantially greater than the range typical for loose sands [e.g., the correlation between cone penetration resistance and relative density for clean sands presented by Idriss and Boulanger (2008) gives q_{cN} values ranging from 53 to 90 at one atmosphere effective overburden stress for relative densities between 30 and 50%], despite having similar cyclic strengths (Price et al. 2017). This difference may be attributed to (1) differences in compressibility and crushability in both compression and shear (there were no measurable changes to the grain size distribution for the 100S silt following one-dimensional compression tests with σ_v' exceeding 100 MPa, whereas there generally are for silica sands), (2) differences in particle shape (the silt is highly angular while most sands have predominately sub-rounded particles) resulting in high peak friction and dilation angles for the 100S silt [e.g., Santamarina and Cho (2004) report critical state friction angles upwards of 40 degrees for highly angular particles], (3) uncertain sensitivity of penetration

resistance for the nonplastic silt to initial density, and (4) ageing and/or depositional anisotropy [owing to the presence of non-spherical particles (Santamarina and Cho 2004)] and associated fabric effects.

The centrifuge model test results and discussion presented herein are for young, slurry deposited idealized mixtures of silica silt and kaolin. Experimental limitations may have impacted the presented results but are likely of little significance with respect to the broader conclusions drawn. As detailed above, the corrections applied for excess pore pressure generation, temperature variation during cone penetration, and load cell resolution and drift were, when possible, consistent with practice and the reasonableness of the corrections checked against available datasets and literature. Vibration of the servo controlled proportional valve regulating the cone actuator (vibrations were likely caused by noise in the feedback system passing through the centrifuge's slip rings) may have also impacted test results; however, parts of and in some cases entire cone soundings that were visibly affected by such behavior were disregarded. Potential boundary effects for cone penetration in the 100S silt, which exhibited strong dilative tendencies (and for which a greater mobilized soil volume during cone penetration can be expected), were not quantified but may have impacted cone penetration measurements.

Summary and Conclusions

A series of centrifuge model tests with variable rate in-flight cone penetration soundings was performed for slurry deposited mixtures of silica silt with 0, 2.5, 5, and 20% kaolin by dry mass (PI ranging from 0 to 6). T-bar penetration soundings for the mixture with 20% kaolin provided independent measurement of the soil's undrained shear strength.

Penetration resistances decreased with increasing clay content for the same drainage condition across the soils tested. The addition of a small amount of clay to the nonplastic silt (from 100S to 97.5S2.5K) resulted in an order of magnitude decrease in both drained and undrained penetration resistances. In addition, penetration resistances in the mixtures with 5 and 20% kaolin decreased with increasing penetration rate, whereas the penetration resistance for the 100S silt increased as penetration rate increased. This difference in the effect of penetration rate was attributed to strong dilative tendencies of the 100S silt.

The results of the centrifuge experiments performed in this study are limited to young, slurry deposited low-plasticity silts. Complexities encountered in natural soils in situ such as age effects and stratigraphic variation (e.g., laminations and thin layer effects; variable local drainage conditions) are not captured by the tests performed in this study. This study (and its supporting works) aim to improve understanding of the behavior of low-plasticity silts and contribute to development of a more unified approach to interpretation of cone penetration test results across a broad range of soils. Theoretical insights regarding the relative contributions of differences in compressibility, dilatancy, and state on the observed differences in penetration resistance across the silt-clay mixtures may be drawn from future numerical studies.

Acknowledgements

Portions of the work presented herein were derived from studies supported by the California Department of Water Resources (contract 4600009751) and the National Science Foundation (grants CMMI-1138203 and CMMI-1300518). Support for the Natural Hazards Engineering Research Infrastructure (NHERI) centrifuge facility at UC Davis was also provided by the National Science Foundation (award CMMI-1520581). Any opinions, findings, or recommendations

expressed in this material are those of the authors and should not be interpreted as necessarily representing the official policies, either expressed or implied, of either organization. Steven Haugaard performed the one-dimensional compression tests presented herein. Mohammad Khosravi, Dan Wilson and the staff of the Center for Geotechnical Modelling at UC Davis supported the experimental design and execution of the centrifuge model tests presented herein. The authors are grateful for the above assistance and support.

Notation

The following symbols are used in this paper:

A_p = T-bar projected tip area;

A_s = T-bar shaft area;

a = cone net area ratio;

B_q = pore pressure parameter;

CRR = cyclic resistance ratio;

CRS = constant rate of strain;

c = parameter describing the rate of change of penetration resistance with velocity;

c_h = horizontal coefficient of consolidation;

c_v = vertical coefficient of consolidation;

DSS = direct simple shear;

d = cone diameter;

f_s = sleeve friction;

IL = incremental load;

u_o = initial hydrostatic pore pressure;

u_2 = pore pressure acting on the cone shoulder;

LL = liquid limit;

m = parameter describing the variation of undrained shear strength ratio with OCR;

N_{kt} = cone strength factor where $s_u = (q_t - \sigma_{vo})/N_{kt}$;

N_{T-bar} = T-bar strength factor where $s_u = (q_{T-bar} - \sigma_{vo})/N_{T-bar}$;

OCR = overconsolidation ratio;

P_a = atmospheric pressure;

PI = plasticity index;

Q = normalized cone tip resistance;

Q_{ref} = reference normalized cone tip resistance for undrained penetration;

q_c = measured cone tip resistance;

q_{cN} = measured cone tip resistance in atmospheres ($q_{cN} = q_c/P_a$);

q_{c_raw} = raw measured tip cone resistance;

q_{cN_raw} = raw measured cone tip resistance in atmospheres ($q_{cN\_raw} = q_{c\_raw}/P_a$);

q_{c1N} = measured cone tip resistance in atmospheres corrected to an effective overburden stress of 1 atm;

q_t = total cone tip resistance;

q_{t_net} = net total cone tip resistance ($q_{t\_net} = q_t - \sigma_{vc}$);

q_{tN} = total cone tip resistance in atmospheres ($q_{tN} = q_t/P_a$);

q_{T-bar} = T-bar penetration resistance;

$q_{T-bar,net}$ = T-bar net penetration resistance ($q_{T-bar,net} = q_{T-bar} - [\sigma_{vc} - u_o(1-\alpha)]\frac{A_s}{A_p}$);

s_u = undrained shear strength;

V = normalized penetration velocity;

V_{50} = normalized penetration velocity at which the cone penetration resistance is half way between the fully drained and undrained values;

v = penetration rate;

α = Ratio of the T-bar load cell core area to the T-bar shaft area;

σ_{vc} = total vertical consolidation stress;

σ'_v = vertical effective stress;

σ'_{vc} = vertical effective consolidation stress; and

τ = shear stress.

References

Bolton, M. D., Gui, M. W., Garnier, J., Corte, J. F., Bagge, G., Laue, J., and Renzi, R. (1999). "Centrifuge cone penetration tests in sand." *Géotechnique*, 49(4), 543-552.

Boulanger, R. W., and Idriss, I. M. (2016). "CPT-based liquefaction triggering procedure." *J. Geotech. Geoenviron. Eng.*, 10.1061/(ASCE)GT.1943-5606.0001388, 0401506.

Chow, S. H., Bienen, B. and Randolph, M. F. (2018). "Rapid penetration of piezocones in sand". *Proc., 4th Int. Symp. On Cone Penetration Testing,* Delft, 213-219.

Chung, S. F., Randolph, M. F., and Schneider, J. A. (2006). "Effect of penetration rate on penetrometer resistance in clay." *J. Geotech. Geoenviron. Eng.*, 132(9), 1188-1196.

DeJong, J. T., and Randolph, M. (2012). "Influence of partial consolidation during cone penetration on estimated soil behavior type and pore pressure dissipation measurements." *J. Geotech. Geoenviron. Eng.*, 10.1061/(ASCE)GT.1943-5606.0000646, 777-788.

DeJong, J. T., Yafrate, N. J., and DeGroot, D. J. (2011). "Evaluation of undrained shear strength using full-flow penetrometers." *J. Geotech. Geoenviron. Eng.*, 10.1061/(ASCE)GT .1943-5606.0000393, 14-26.

Haugaard, S., Price, A., DeJong, J. T., and Boulanger, R. W. (2018). One-dimensional compression and consolidation test results. DesignSafe-CI [publisher], Dataset, dx.doi.org/10.17603/DS24964

Idriss, I. M., and Boulanger, R. W. (2008). *Soil liquefaction during earthquakes*. Monograph MNO-12, Earthquake Engineering Research Institute, Oakland, CA, 261 pp.

Jaeger, R. A., DeJong, J. T., Boulanger, R. W., Low, H. E., and Randolph, M. F. (2010). "Variable penetration rate CPT in an intermediate soil." *Proc., 2nd Int. Symp. on Cone Penetration Testing,* Huntington Beach, CA, paper 2-50.

Krage, C. P., Price, A. B., Lukas, W. G., DeJong, J. T., DeGroot, D. J., and Boulanger, R.W. (2018). "Slurry deposition method of low plasticity intermediate soils for laboratory element testing." *Geotech. Test. J.* (submitted).

Kutter, B. L. (1995). "Recent Advances in Centrifuge Modeling of Seismic Shaking." State of the Art Paper, *Proc., 3rd International Conference on Recent Advances in Geotechnical Earthquake Engineering and Soil Dynamics*, St. Louis, MO, Vol. 2, April 199

Lunne, T. (1997). *Cone Penetration Testing in Geotechnical Practice*, CRC Press, London.

Price, A. B. (2018). "Cyclic Strength and Cone Penetration Resistance for Mixtures of Silica Silt and Kaolin." Doctoral dissertation, University of California, Davis.

Price, A. B., Boulanger, R. W., and DeJong, J. T. (2018a). Centrifuge modeling of variable rate cone penetration in low-plasticity silts. DesignSafe-CI [publisher], Dataset, dx.doi.org/10.17603/DS2J67J

Price, A. B., DeJong, J. T., and Boulanger, R.W. (2017). "Cyclic loading response of silt with multiple loading events." *J. Geotech. Geoenviron. Eng.*, 10.1061/(ASCE)GT.1943-5606 .0001759, 04017080.

Price, A. B., DeJong, J. T., Boulanger, R. W. (2018b). Direct simple shear testing for silica silt and kaolin mixtures. DesignSafe-CI [publisher], Dataset, dx.doi.org/10.17603/DS2SQ30

Randolph, M. F. (2004). "Characterisation of soft sediments for offshore applications." *Proc., Int. Conf. Geotechnical Geophysical Site Characterization*, ISC-2, Millpress, The Netherlands, 209–232.

Randolph, M. F., and Hope, S. (2004). "Effect of cone velocity on cone resistance and excess pore pressures." *Proc., IS Osaka-Engineering Practice Performance Soft Deposits*, Osaka, Japan, 147–152.

Robertson, P. K. (1990). "Soil classification using the cone penetration test." *Can. Geotech. J.*, 27(1), 151-158.

Santamarina, J. C., and Cho, G. C. (2004). "Soil behaviour: The role of particle shape." *Advances in Geotechnical Engineering: The Skempton Conference*, Vol. 1, Thomas Telford, London, 604-617.

Schneider, J. A., Lehane, B. M., and Schnaid, F. (2007). "Velocity effects on piezocone measurements in normally and over consolidated clays." *Int. J. Phys. Model. Geotech.*, 7(2), 23-34.

Schneider, J. A., Randolph, M. F., Mayne, P. W., and Ramsey, N. R. (2008). "Analysis of factors influencing soil classification using normalized piezocone tip resistance and pore pressure parameters." *J. Geotech. Geoenviron. Eng.*, 10.1061/(ASCE)1090-0241 (2008)134:11(1569), 1569-1586.

Silva, M F. (2005). "Numerical and physical model of rate effects in soil penetration." Doctoral dissertation, King's College, University of Cambridge, Cambridge, UK.

Silva, M. F., White, D. J., and Bolton, M. D. (2006). "An analytical study of the effect of penetration rate on piezocone tests in clay." *Int. J. Numer. Anal. Methods Geomech.*, 30(6), 501-527.

Suzuki, Y. and Lehane, B. M, (2014). "Rate dependence of q_c in two clayey sands". *Proc., 3rd Int. Symp. on Cone Penetration Testing,* Las Vegas, Nevada, 411-418.

White, D. J., Gaudin, C., Boylan, N., and Zhou, H. (2010). "Interpretation of T-bar penetrometer tests at shallow embedment and in very soft soils." *Can. Geotech. J.*, 47(2), 218-229.

Figures

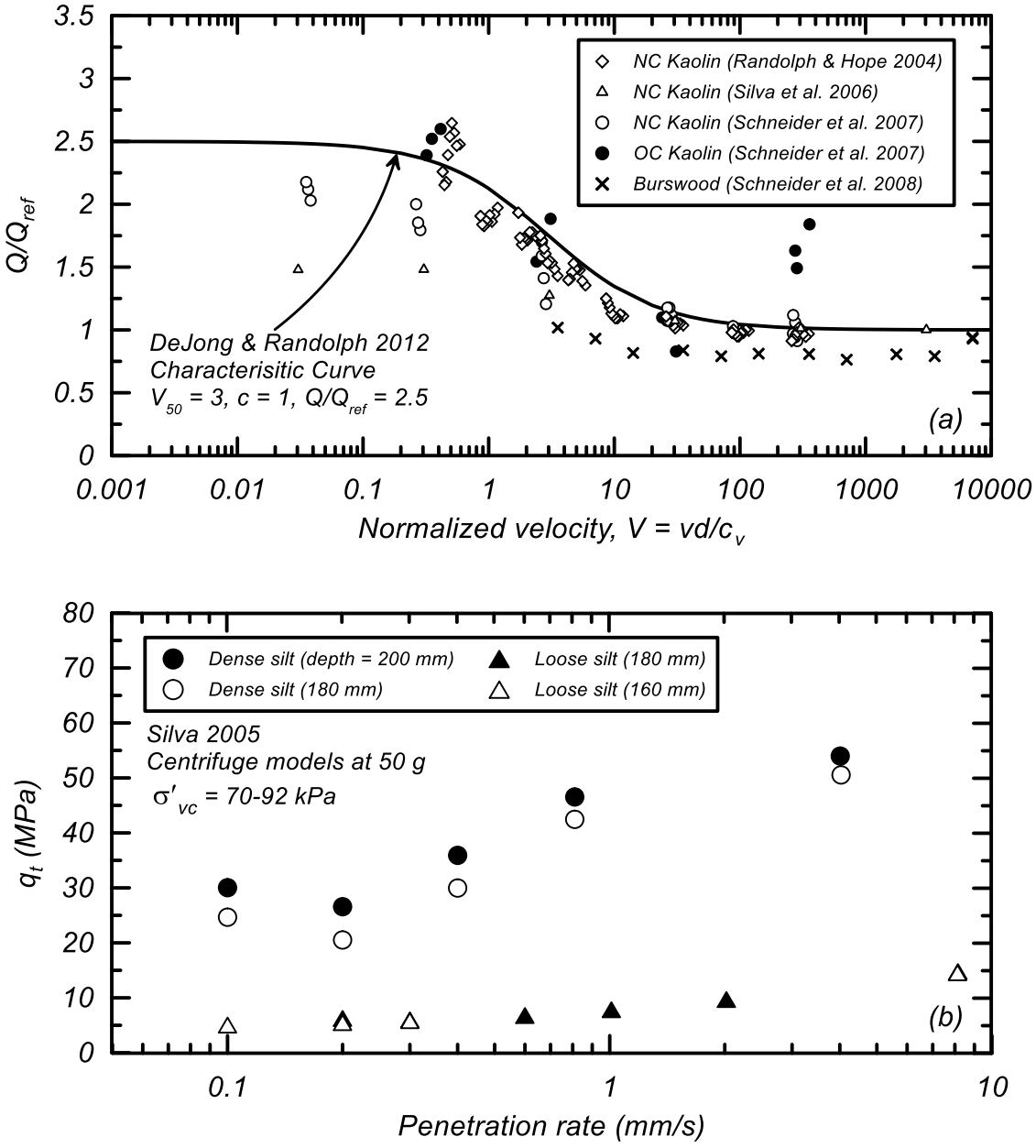

Fig. 1. Experimental variable rate cone penetration studies in: (a) clays; (b) nonplastic silica silt

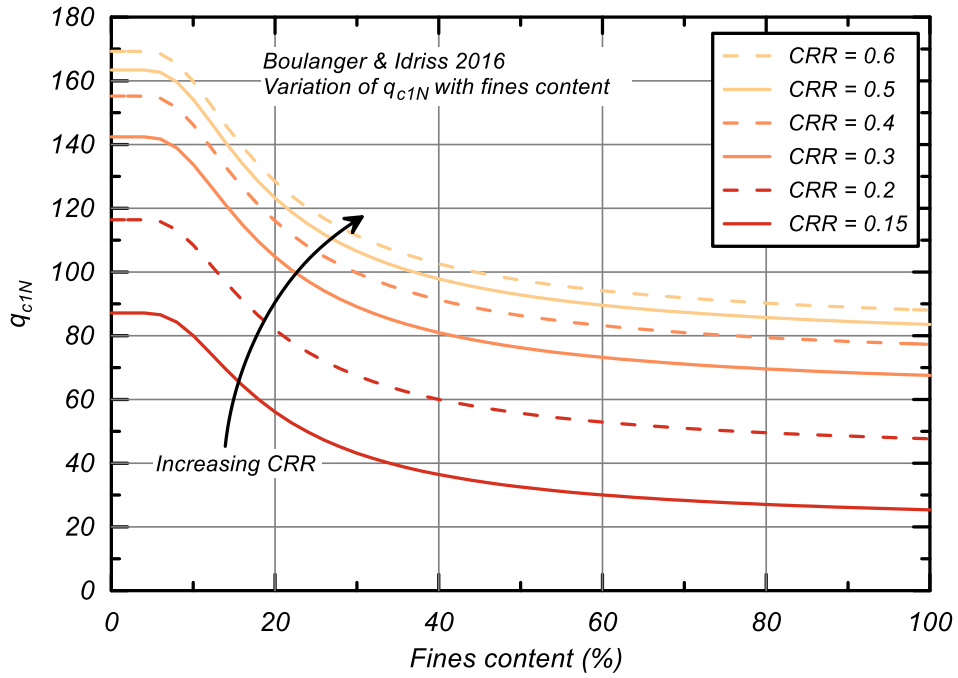

Fig. 2. Variation in q_{c1N} with fines content for a given CRR value based on a case history-based liquefaction triggering correlation

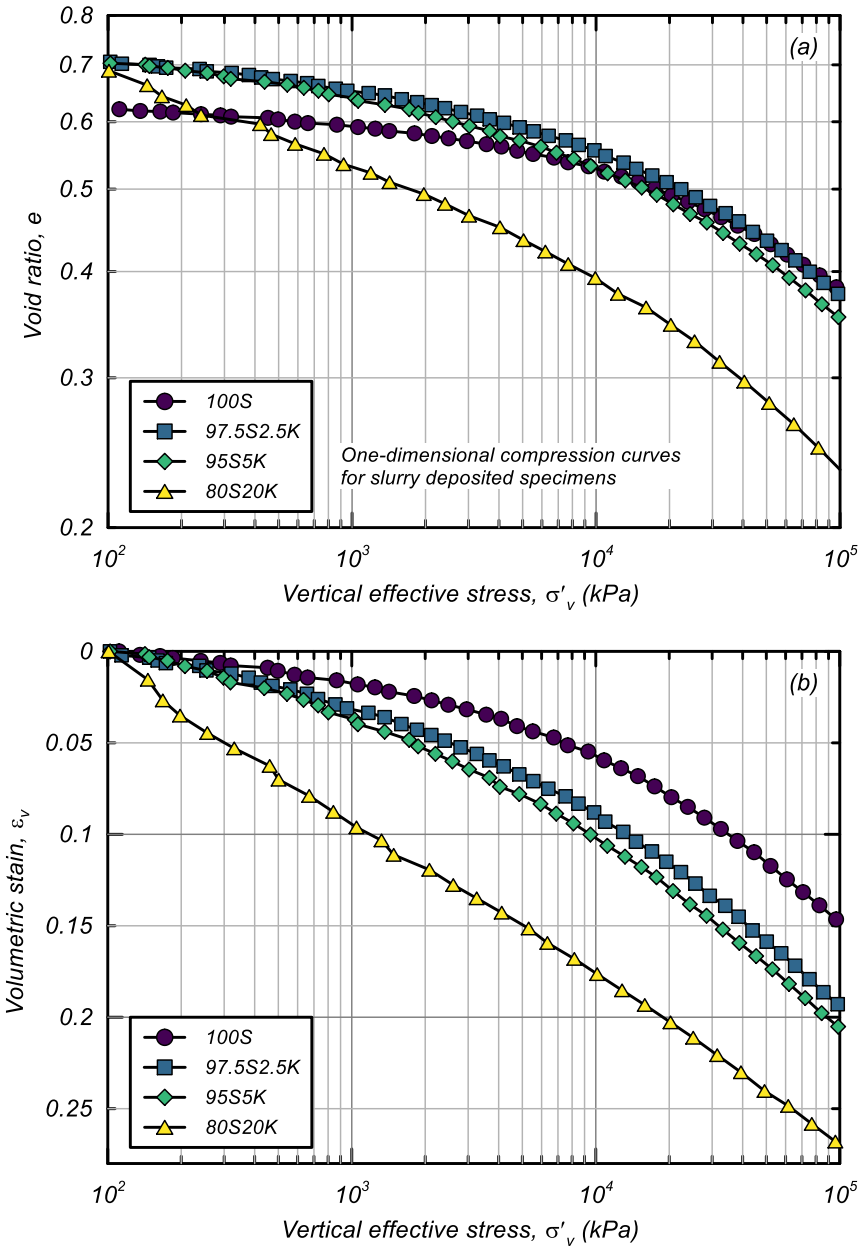

Fig. 3. One-dimensional compression test results: (a) void ratio versus vertical effective stress; (b) volumetric strain versus vertical effective stress

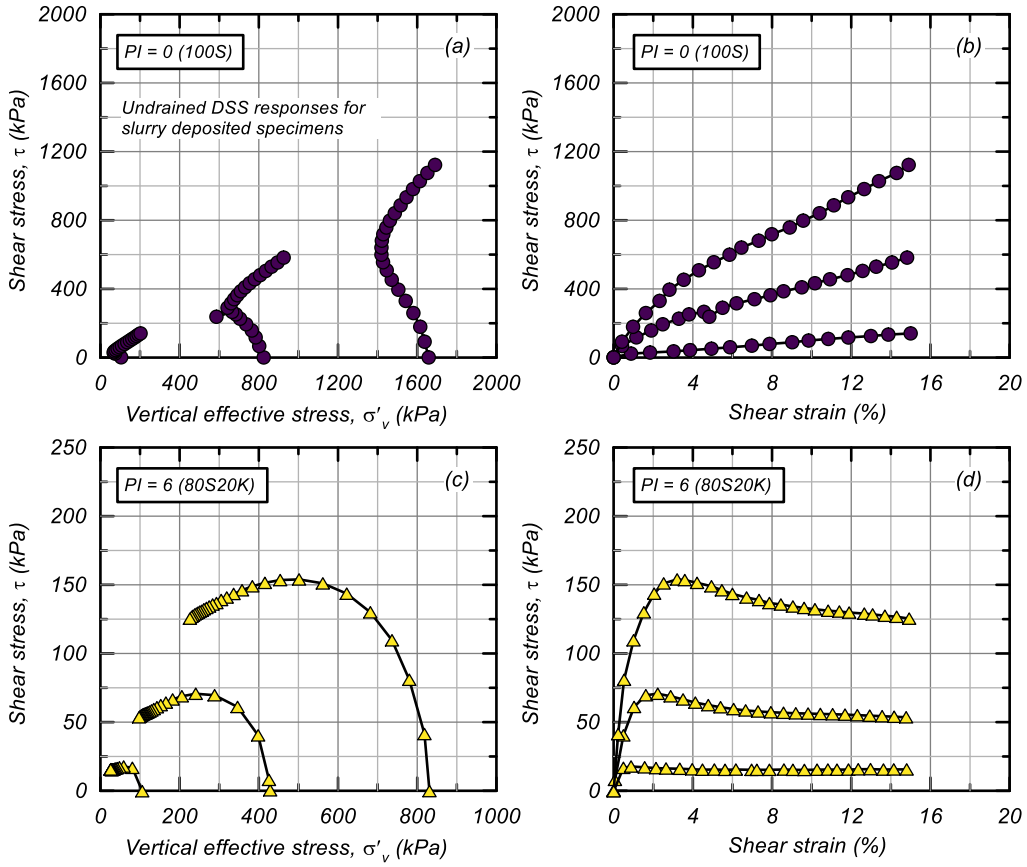

Fig. 4. Undrained monotonic DSS responses for three levels of confinement: (a and b) 100S silt; (c and d) 80S20K mixture

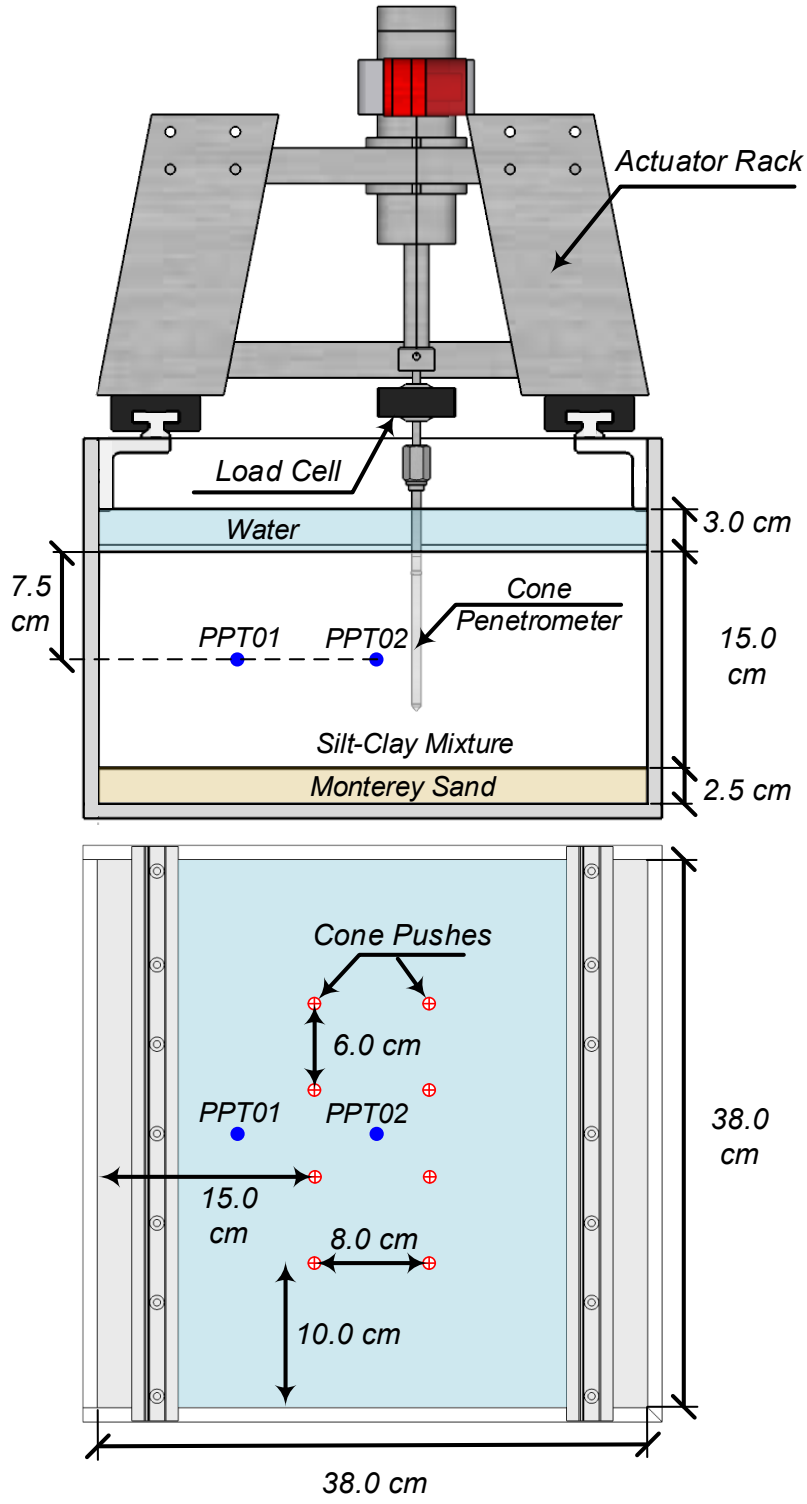

Fig. 5. Plan and cross-sectional model views with typical cone sounding and sensor locations

Fig. 6. Centrifuge model construction: (a) vacuum slurry mixer; (b) mixed 97.5S2.5K slurry; (c) pre-consolidated 80S20K model; (d) slurry deposition of the 97.5S2.5K mixture; (e) slurry deposition of the 95S5K mixture; (f) slurry deposition of 100S silt; (g) 6-mm cone penetrometer and actuator rack; (h) silt model with cone actuator rack on 1-m radius centrifuge

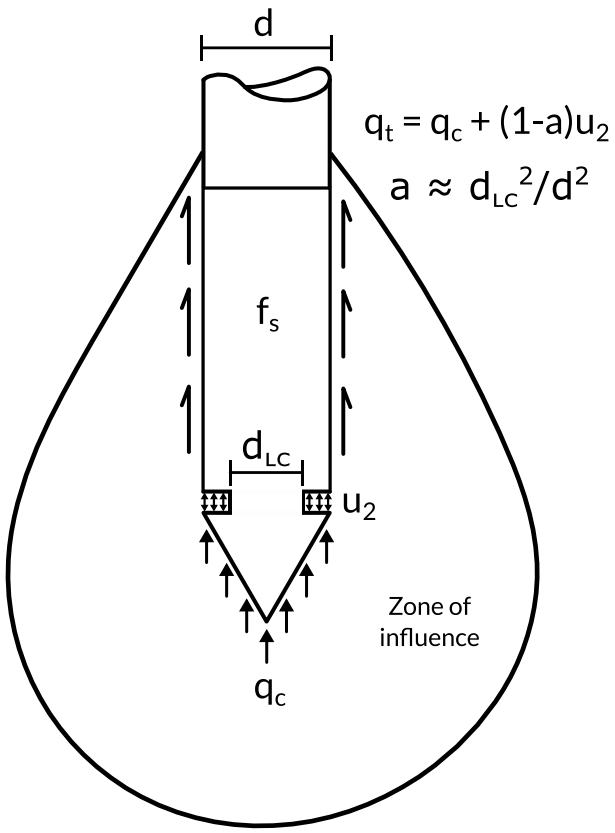

Fig. 7. Schematic of pore pressure correction for cone penetration test results (q_c is the measured cone tip resistance; $u_2$is the pore pressure acting on cone shoulder; d_{LC} is the diameter of the load cell support; d is the cone diameter; f_s is the sleeve friction; a is the net area ratio; q_t is the total cone resistance)

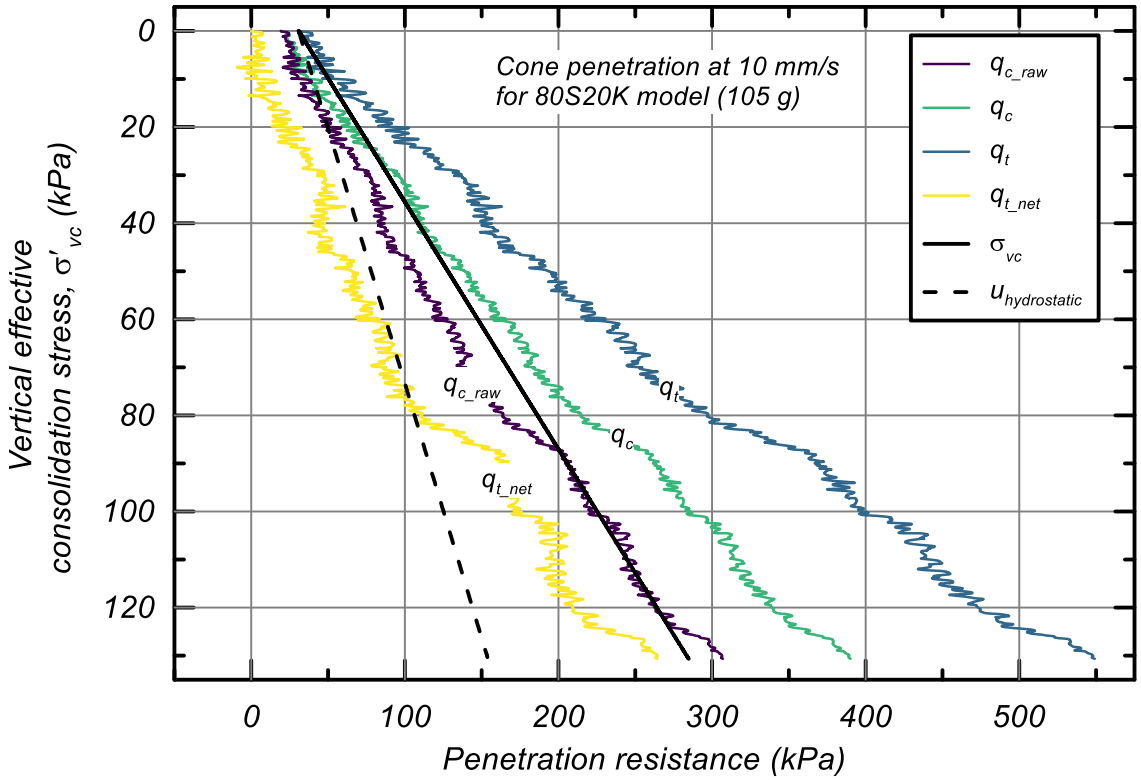

Fig. 8. Cone penetration test results for the 80S20K mixture for a penetration rate of 10 mm/s illustrative of the temperature and pore pressure corrections

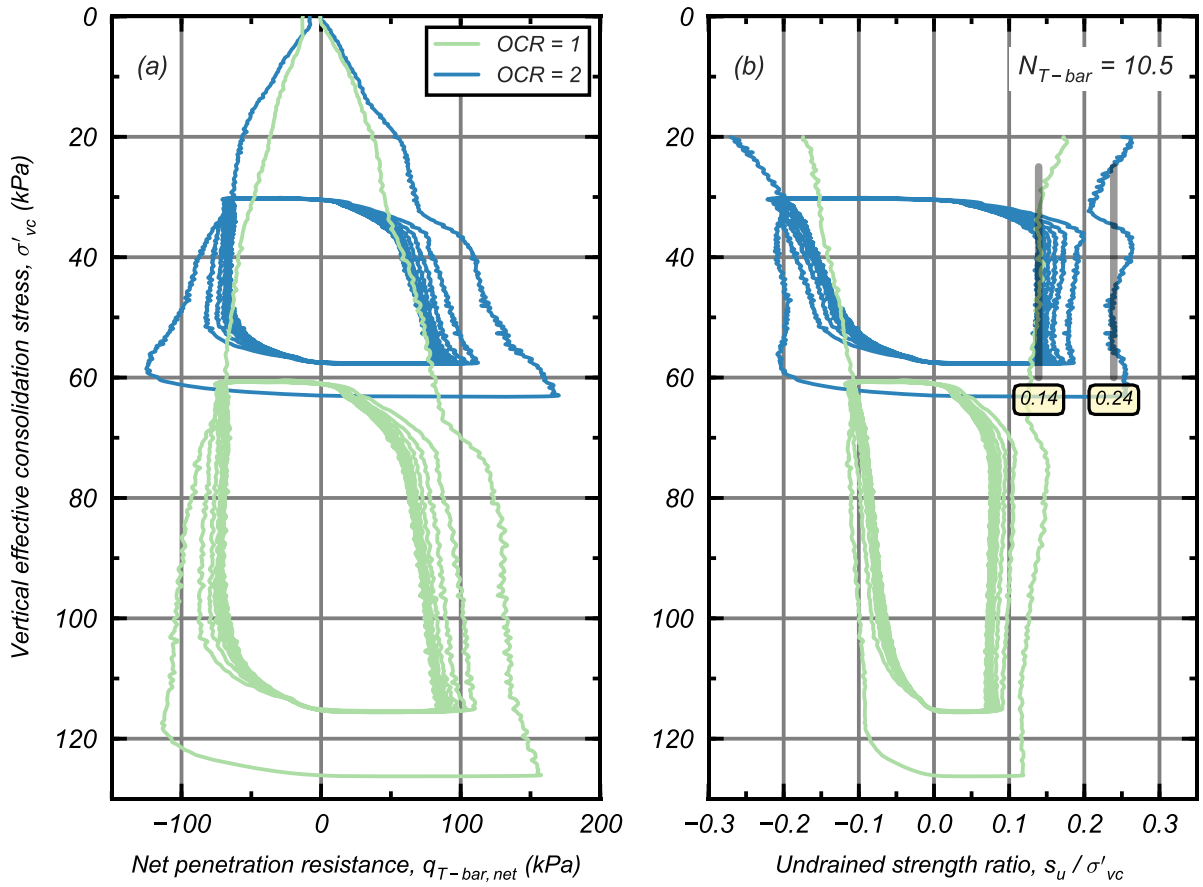

Fig. 9. Cyclic T-bar penetration soundings for the 80S20K mixture for OCR = 1 (105 g) and OCR = 2 (53 g): (a) profiles of net penetration resistance; (b) profiles of normalized undrained shear strength with average undrained strength ratios over a common vertical effective stress interval (25 to 60 kPa) of 0.14 and 0.24 for OCR = 1 and 2, respectively

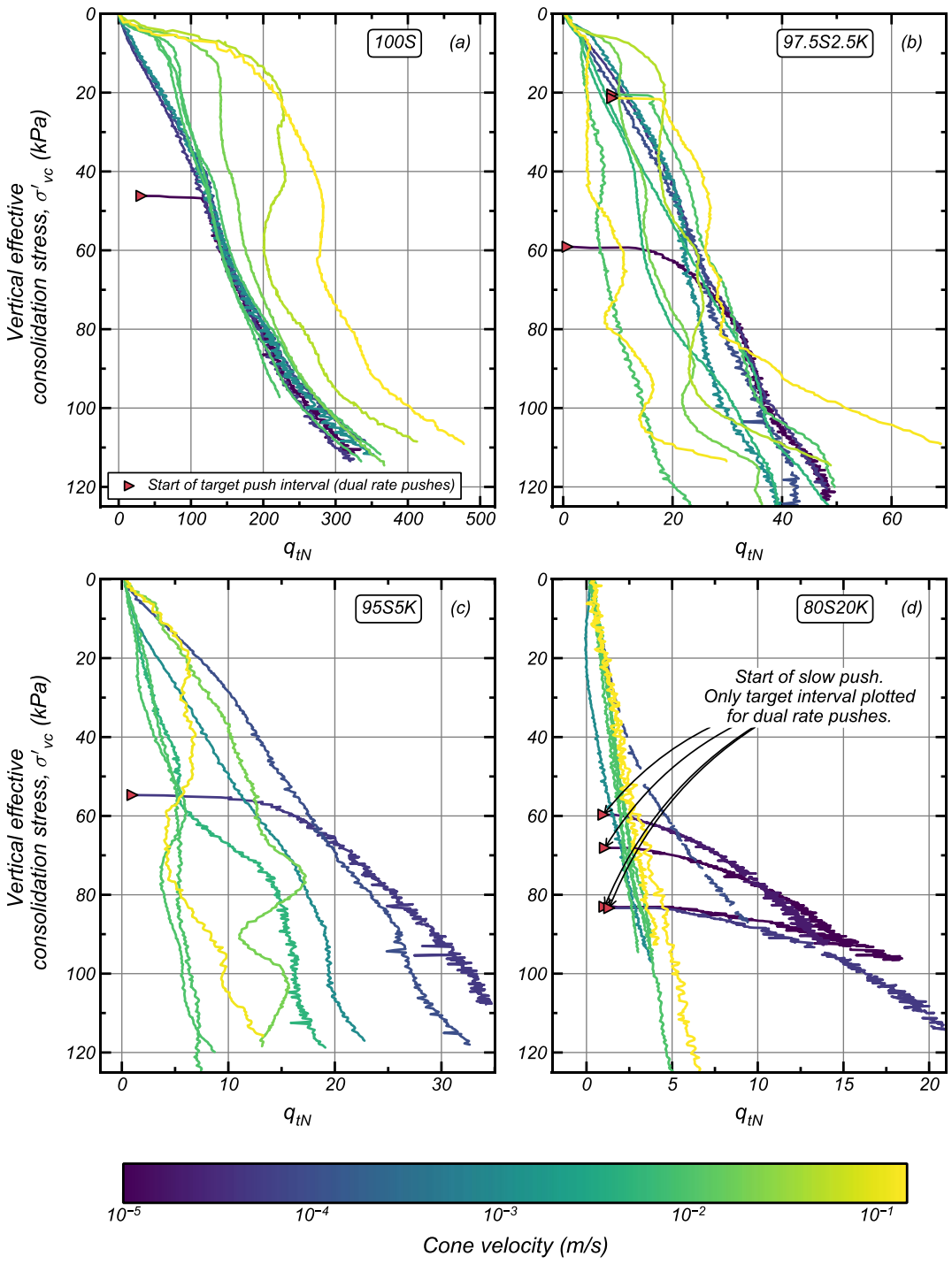

Fig. 10. Cone penetration resistance profiles for the four silt-clay mixtures (note that the scale for penetration resistance changes between plots): (a) 100S; (b) 97.5S2.5K; (c) 95S5K; (d) 80S20K

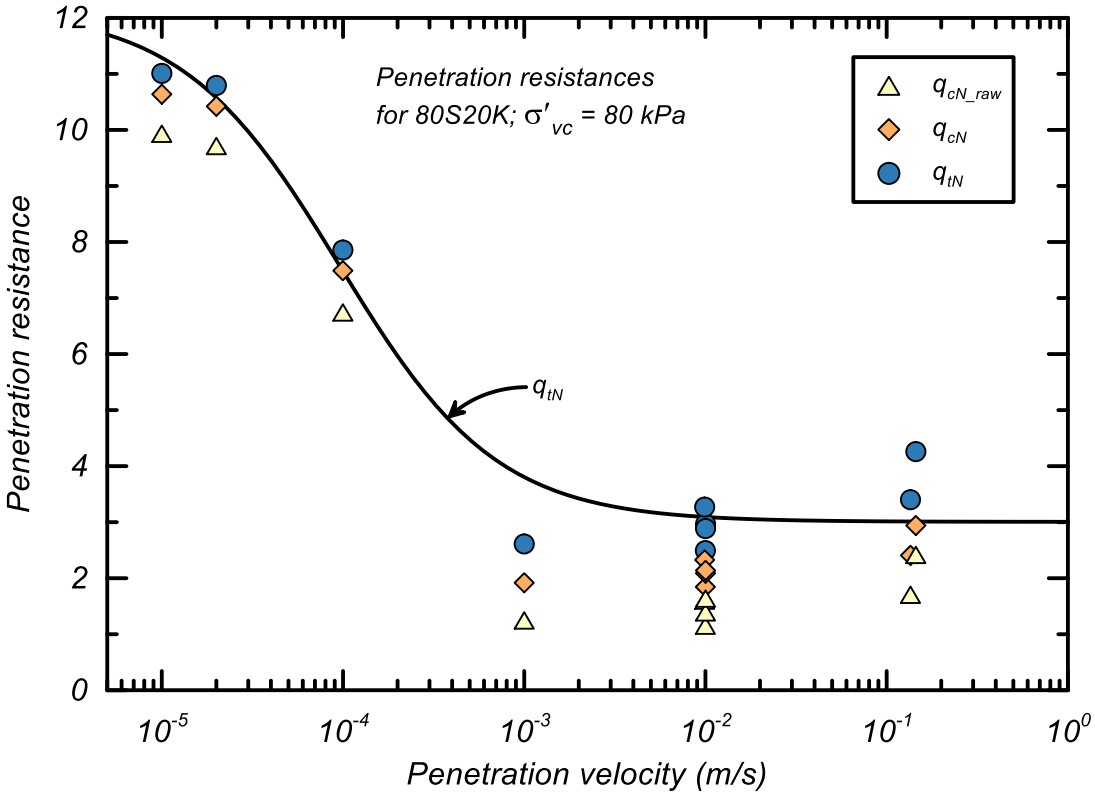

Fig. 11. Pore pressure and temperature corrections for the 80S20K silt-clay mixture

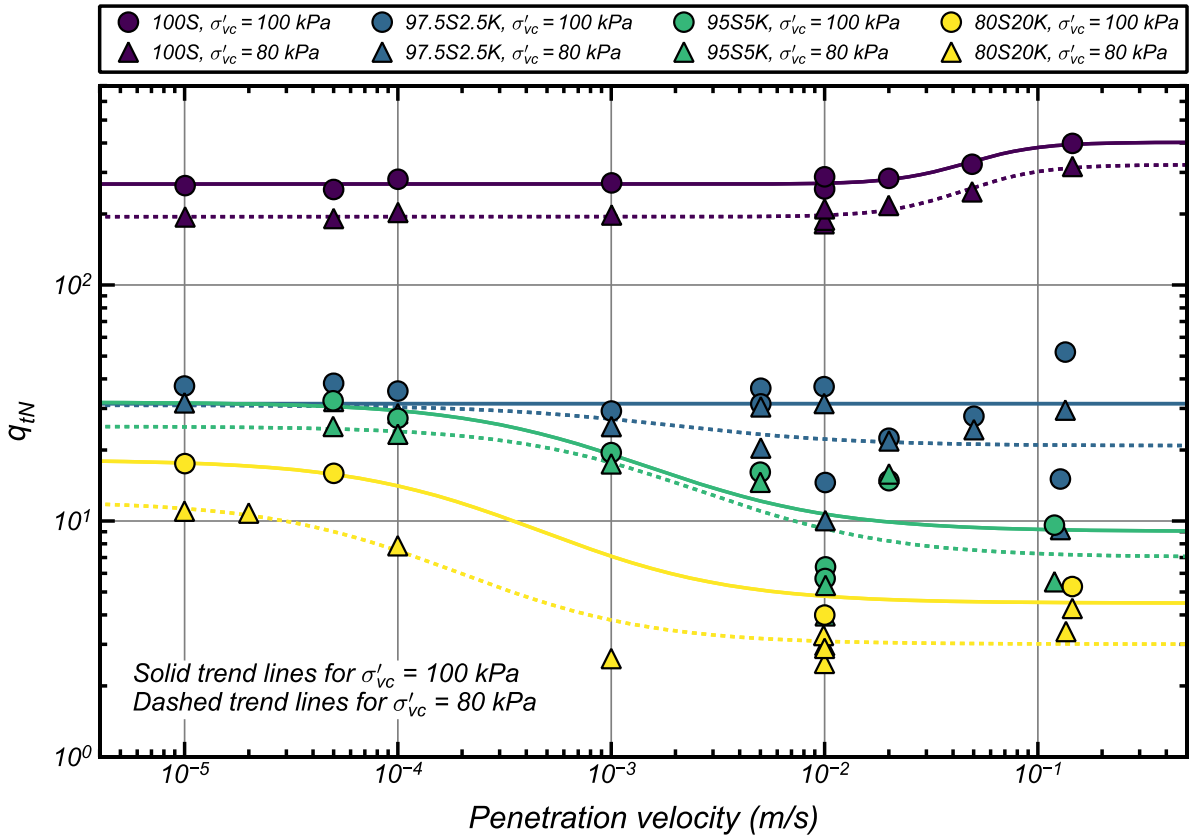

Fig. 12. Cone penetration resistance versus penetration velocity

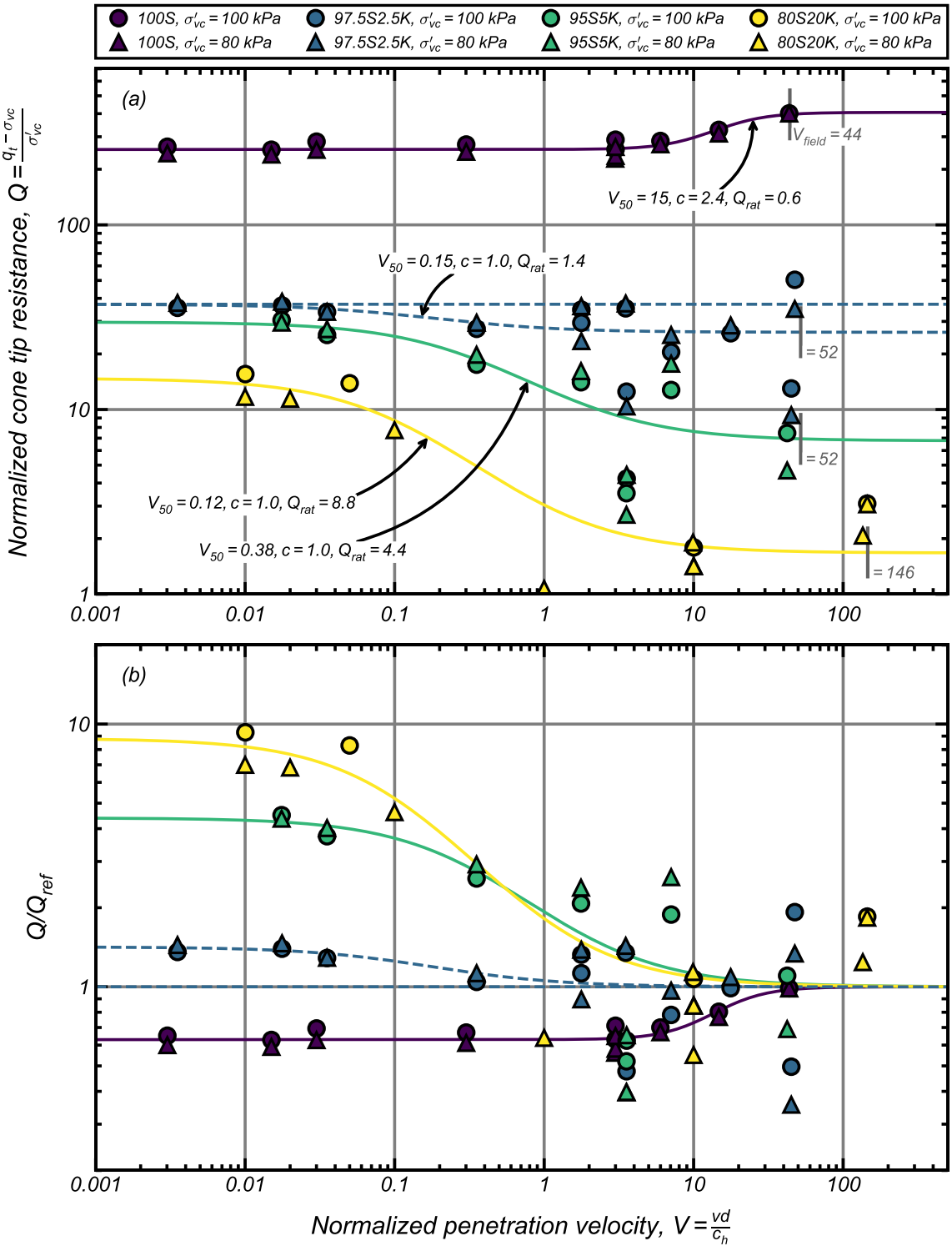

Fig. 13. Cone penetration resistance versus normalized penetration velocity: (a) Q vs. V; (b) Q/Q_{ref} vs. V

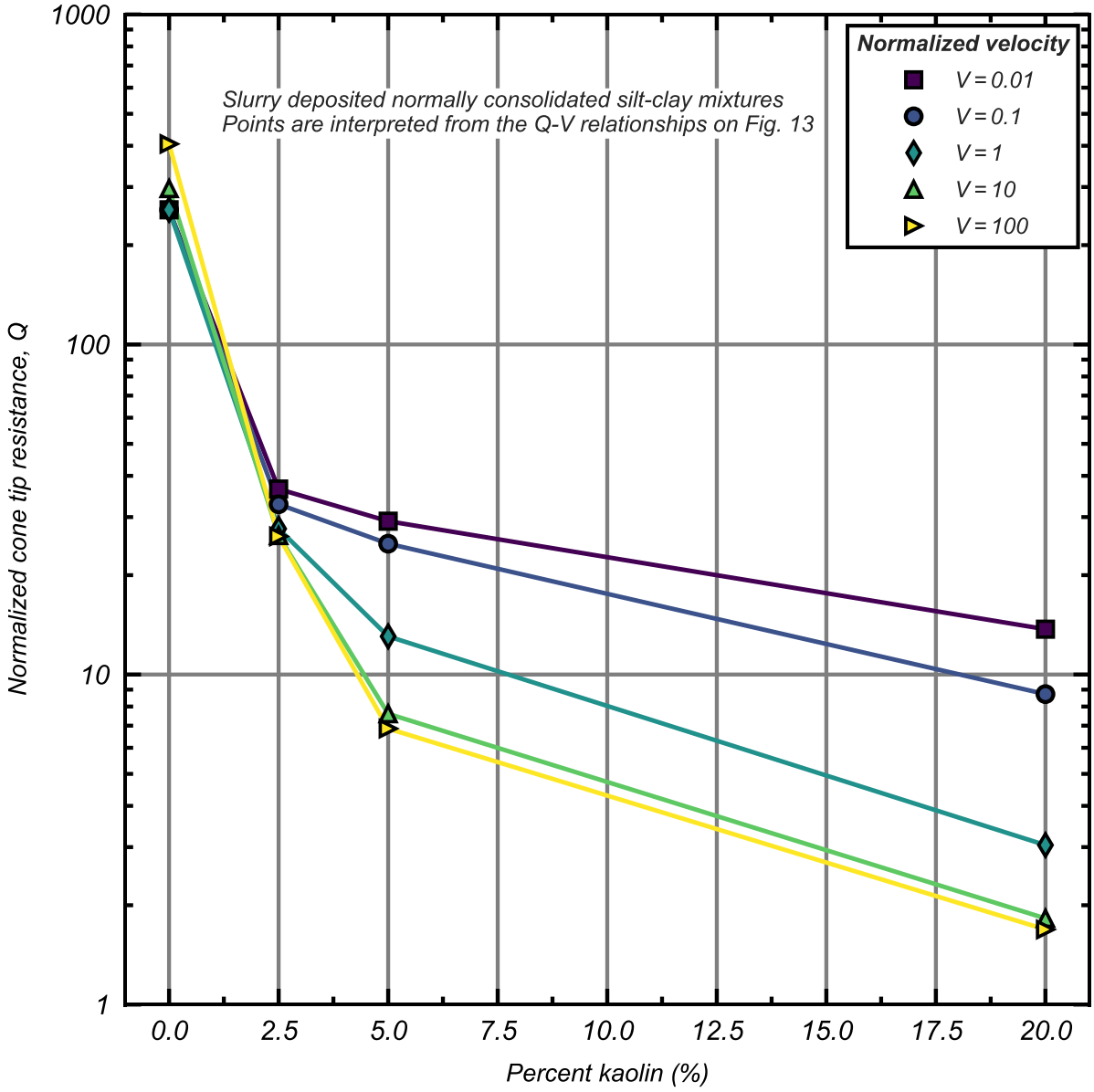

Fig. 14. Variation of penetration resistance with clay content